EFDA–JET–CP(08)05/15

W. Fundamenski, R.A. Pitts, G. Arnoux, M. Jakubowski, A. Loarte,
M. Beurskens and JET EFDA contributors

ELM Filament Heat Loads on Plasma Facing Components in JET and ITER

ELM Filament Heat Loads on Plasma Facing Components in JET and ITER

W. Fundamenski[1], R.A. Pitts[2], G. Arnoux[1], M. Jakubowski[3], A. Loarte[2], M. Beurskens[1] and JET EFDA contributors*

JET-EFDA, Culham Science Centre, OX14 3DB, Abingdon, UK

[1]EURATOM-UKAEA Fusion Association, Culham Science Centre, OX14 3DB, Abingdon, OXON, UK
[2]ITER Organistion, CEN Cadarache, 523/27, 13108 St.Paul-Lez Durance, France
[3]Max-Planck Institut fur Plasmaphysic, IPP-Euratom Association, D-85748 Garching, Germany
** See annex of F. Romanelli et al, "Overview of JET Results",*
(Proc. 22[nd] IAEA Fusion Energy Conference, Geneva, Switzerland (2008)).

Preprint of Paper to be submitted for publication in Proceedings of the
22nd IAEA Fusion Energy Conference, Geneva, Switzerland.
(13th October 2008 - 18th October 2008)

ABSTRACT.
Observations of localized heat loads to ELM filament impact on the main chamber in JET are reviewed and drawn together to form a coherent picture of the exhaust phase of the ELM. Presently available JET data is quantitatively explained by a parallel loss model of ELM filament dynamics, in which the evolution of filament density and temperature proceeds via a competition of radial advection and parallel convective and conductive losses. The fraction of ELM energy reaching the wall increases with ELM amplitude, in rough agreement with a modified interchange scaling of filamentary motion. The model validated on JET data predicts that ~25% and ~4% of the ELM energy would reach the main chamber (mostly the upper baffle) in ITER for natural (20MJ, $\Delta W/W_{ped} \sim 13.3\%$) and mitigated (1MJ, $\Delta W/W_{ped} \sim 0.66\%$) ELMs, respectively.

1. INTRODUCTION

It is now widely recognised that Type-I ELMs generate filamentary structures which travel radially well into the far Scrape-Off Layer (SOL). The localised heat loads on Plasma Facing Components (PCFs), including the divertor, limiter and upper dump plate tiles, associated with such ELM filaments are one of the critical issues for ITER; specifically, main chamber PFCs in ITER are presently being redesigned with the aim of handling such plasma related heat loads. Since their earliest observations, the kinematics, dynamics and dissipation of Type-I ELM filaments (i.e. their radial motion, driving forces and parallel loss mechanisms), as well as the resulting heat loads on the vessel wall, have been a topic of active research on JET. In this contribution, the results of this activity are briefly reviewed, leading to ITER predictions.

2. ELM FILAMENT HEAT LOADS ON JET

Type-I ELM-filaments are observed on JET using both visible (D±) and wide angle infra-red cameras; Type-III ELM filaments do not to leave a measurable heat loads imprint on main chamber PFCs. In all cases analysed, ELM filaments are found to follow pre-ELM magnetic field lines, i.e. they did not noticeably distort/perturb the SOL (poloidal/toroidal) magnetic field, see Fig.1. This agreement between the pitch angle of ELM filament heat load imprint and that of the pre-ELM magnetic field line (at the point of contact with the wall) is observed in both low and high triangularity (ITER-like shape) discharges, and in the latter, at both on the upper dump plate and on the outboard limiters [6] (of course, the pitch angle varies by more than a factor of 5 between these two locations, being much shallower near the upper dump plate due to the proximity of the second X-point).

In the high triangularity plasmas, the toroidal separation, $\Delta\phi \sim 2\pi/n_w$, where n_w is the inferred number of filaments at the wall radius (or the quasi-toroidal mode number), was found as follows [6], Fig.2: (a) $n_w \sim 30-40$ at the outer limiter ($\Delta r = r - r_{sep} \sim 5$cm), with little dependence on ELM size, Fig.2(a); (b) $n_w \sim 60-20$ at the upped dump plate ($\Delta r \sim 2$cm). The latter exhibited roughly inverse linear dependence on ELM size, Fig.2(b), albeit, due to a significant scatter in n_w for a given ΔW_{ELM}, it should be treated with some caution. In both cases, the relative width, $\delta\theta/\Delta\theta$, is

$$n_w \approx 6\left(\frac{\Delta W_{ELM}}{W_{ped}}\right)^{-1} \quad (1)$$

roughly independent of ELM size, with an average value of $\delta\theta/\Delta\theta \sim 0.6 \pm 0.2$ at the upper dump plates and $\sim 0.8 \pm 0.2$ at the outer limiters. The observed range of toroidal mode numbers is somewhat higher than predicted by the linear MHD (Peeling-Ballooning) model of the ELM instability, in which modes with $n_0 \sim 5-20$ are most unstable, suggesting break-up of initial ELM filaments into a few (~3) smaller fragments in the SOL, i.e. before hitting the wall; such fragmentation of a filament into roughly three smaller pieces is consistent with recent numerical simulations of interchange driven filamentary structures [Garcia06]. Accepting the P-B prediction of the initial number of filaments, n_0, one may then postulate that $n_w/n_0 \sim 3$ and hence $n_0 \sim 2/(\Delta W_{ELM}/W_{ped})$.

Let us next consider the absolute value of the ELM heat loads to the main chamber wall as a result of the ELM filament impact. The fraction of ELM energy deposited on the wall for a given ELM amplitude and separatrix-to-wall distance has been reasonably well described by a so-called *parallel loss model* of ELM exhaust, Table 1 [2]. This model describes the radial motion of the pedestal plasma as an *effective* filament, moving with some mean radial velocity (which has been obtained from experiment) and subject to parallel losses to the divertor tiles. The filament density and temperature are evolved using the fluid approximation, which although clearly not valid in the initial phase of ELM filament evolution, when free-streaming of Maxwellian ions dominates, is more appropriate to the latter, collisional phase. Moreover it explains some basic features of ELM losses based on the ratio of convective, $\tau_n \sim L_{//}/c_S$, and conductive, $\tau_T \sim L_{//}^2/\chi_e$, parallel loss times, e.g. it predicts mainly conductive losses at low ν^*, when the plasma cools faster than it rarefies ($\tau_n >> \tau_T$), and mainly convective losses at high ν^*, when cooling and rarefication are comparable ($\tau_n \sim \tau_T$), i.e. it explains why small (collisional) ELMs are mainly convective.

The parallel loss model has been successful at reproducing a range of ELM filament measurements on JET, see Table 1, including (i) the fraction of ELM energy deposited on the outer limiters (as measured by infra-red thermography, and also observed as energy missing from the divertor), which is typically ~10% for nominal Type-I ELMs; (ii) the radial efolding lengths of density, electron temperatures and energy, $\lambda_n^{ELM} \sim 12$cm, $\lambda_{Te}^{ELM} \sim 3$cm, and $\lambda W_{ELM} \sim 3.5$cm inferred from dedicated outer gap-scan experiment for medium sized ($\Delta W/W_{ped} \sim 12\%$) Type-I ELMs using the measured SOL-averaged radial filament velocity of $V_\perp^{ELM} \sim 600$m/s [3], and (iii) the far SOL ELM ion energies on JET, measured using a retarding field analyser probe head on fast scanning assembly, which indicate that $\lambda_{Ti}^{ELM} \sim 8$cm [9]. Recently, the model has also been compared against infra-red measurements of ELM filament heat loads on the outboard limiters for discharges with well characterized pedestal density and temperature profiles, see Table 2 and Figure 3. Starting from the inter-ELM pedestal profiles, Fig.3(a), obtained using high resolution Thomson scattering for Pulse No: 70224 and taking the SOL-averaged radial filament velocity at the value previously measured on JET under comparable conditions as $V_\perp^{ELM} \sim 600$m/s (see above), the radial evolution of the fraction of ELM released

energy reaching a given radial location, W'(r) = W(r)/W(0) where W(0) = ΔW_{ELM}, has been calculated for different initial filament positions (pedestal-top, mid-pedestal and separatrix) and radial velocities (600m/s and 1200m/s), Fig.3(b). With the default model assumptions (initial position at mid-pedestal, $V_{\perp}^{ELM}$ ~ 600m/s), the model predicts 9.4% of the ELM energy reaching the wall, in excellent agreement (in view of a range of approximations) with the measured value of 8.8%.

Another important observation, against which this model must be tested is the direct measurement of the pedestal plasma *ne* and *Te* evolution and formation of filaments during an ELM. Such measurements on JET, indicate that for nominal Type-I ELM conditions (ΔW_{ELM} ~100kJ), the inferred energy density in a single filament observed at ~ 5-7cm from the pedestal top, i.e. 1-3cm in the SOL, is roughly 3kJ; here the radial size of the filament was measured as $l_{\perp}$ ~5cm, the poloidal is taken as $l_{\wedge} \sim 3l_{\perp} \sim 15$cm, a uniform distribution of n_e, T_e and $T_i \sim 2T_e$ along its length of $2\pi Rq_{95}$ ~ 50m is assumed [1]. If ten such filaments are present ($n_0 \sim 10$), then their energy content at $r - r_{ped}$ ~ 5-7cm is 30kJ, or ~30% of the ELM. This is in fair agreement with model predictions (with same assumptions as above), Fig.3(b), which predicts ~20-30% of the released ELM energy at that radial location.

Crucially, the fraction of ELM energy observed at the limiters ($r \sim 5$cm) increases with relative ELM size, e.g. from ~ 5% for $\Delta W \sim 250$kJ ($\Delta W/W_{ped} \sim 0.09$) to ~ 10% for $\Delta W \sim 500$kJ ($\Delta W/W_{ped}$ ~ 0.18) [11], see Table 2; similar conclusions have been drawn earlier based on the deficit of the ELM energy reaching the divertor targets [8, 10]. This observation suggests that smaller ELM filaments travel slower, i.e. have a lower radial Mach number, since for dominant convective losses, as appropriate to the far-SOL, one finds

$$\frac{w^{ELM}}{L_{//}} \qquad \frac{V_{\perp}^{ELM}}{c_s} = M_{\perp}^{ELM}, \qquad f_{wall}^{ELM} = \frac{W_{wall}^{ELM}}{\Delta W_{ELM}} \qquad exp\left(-\frac{0.5\Delta_{ped} + \Delta_{SOL}}{w^{ELM}}\right) \tag{2}$$

where λ_W^{ELM} is the (SOL-averaged) decay length of ELM filament energy, and f_{wall}^{ELM} is the fraction of the ELM energy reaching the wall. Interchange dynamics, which are expected to dominate the ELM filament motion, predict that $M_{\perp}$ should increase as the square-root of the perpendicular filament size and the relative pressure perturbation [5],

$$M_{\perp}^{int} = \frac{V_{\perp}^{int}}{c_S} = \left(\frac{2l}{R}\frac{\Delta p}{p0}\right)^{1/2} \tag{3}$$

where l is the perpendicular size of the filament, R is the major radius, Δp is the pressure perturbation due to the filament and p_0 is the background pressure. The perpendicular size of the filament may be related to the relative ELM amplitude, $\Delta W_{ELM}/W_{ped}$, as follows,

$$\frac{W_{ELM}}{W_{ped}} = \frac{V}{V} = \frac{2\pi\kappa a}{\pi\kappa a^2}\frac{r}{} = 2\frac{r}{a} \qquad \frac{W_{fil}}{W_{ped}} = \frac{V_{fil}}{V} = \frac{2qa\kappa}{\pi\kappa a^2}\frac{r}{}\frac{\theta}{} = \frac{\phi}{\pi}\frac{r}{a} = \frac{2}{n_0}\frac{r}{a} = \frac{1}{n_0}\frac{W_{ELM}}{W_{ped}} \tag{4}$$

where $W_{ped} = 3/2 \times p_{ped}V$, $\Delta W_{ELM} = 3/2 \times p_{ped}V$, and $W_{fil} = 3/2 p_{ped}V_{fil}$ are the pedestal, ELM and

ELM filament energies, respectively, V, V and V_{fil} are the plasma, ELM-affected and filament volumes, Δr and a are the ELM-affected and plasma minor radii, $m_0 = 2\pi/\Delta\theta$ and $n_0 = 2\pi/\Delta\phi$ are the initial poloidal and toroidal mode numbers of the ELM, $q = m_0/n_0$ is the safety factor and κ is the plasma elongation (typically q ~ 3 and $\kappa < 1.5$). Since the scaling (3) was derived for a circular, Gaussian filament shape, $\exp(-(x/l)^2)$, one is justified in treating the size scaling as a free parameter, i.e.

$$l \approx l_{\perp}^{\gamma} l_{\wedge}^{1-\gamma} \approx (\quad r)^{\gamma} (a \quad \theta)^{1-\gamma} \tag{5}$$

where $\gamma = 0.5$ corresponds to equal scaling with radial and poloidal widths and $\gamma = 0$ to a purely poloidal scaling; since the poloidal gradient is the main driving term [5], the latter choice ($\gamma = 0$) may be taken as the default Ansatz. However, equation (1) implies that

$$\frac{l_{\perp}}{a} \quad \frac{c_{\perp} \quad r}{a} \approx \frac{3c_{\perp}}{n_w} \approx \frac{c_{\perp}}{n_0}, \quad \frac{l_{\wedge}}{a} \approx \frac{c_{\wedge} a\kappa \quad r\theta}{a} \approx \frac{2\pi\kappa c_{\wedge}}{n_0 q}, \qquad \frac{l_{\wedge}}{l_{\perp}} \approx \frac{2\pi\kappa c_{\wedge}}{q c_{\perp}} \approx 3\frac{c_{\wedge}}{c_{\perp}} \sim 3 \tag{6}$$

where $c_{\perp}$ and $c_{\wedge}$ are assumed to be comparable, so that the *initial* filament aspect ratio, $l_{\wedge}/\, l_{\perp}$, is independent of n_0 and hence of $\Delta W_{ELM}/W_{ped}$. A similar result, with $l_{\wedge}/\, l_{\perp} \sim 3$, was also obtained based on measurements of $l_{\wedge}$ and $l_{\perp}$ on several tokamaks [7]; this agreement can be interpreted as supporting evidence for the inverse scaling in equation (1), which was based on data with a relatively high scatter. It is interesting to note that the JET infra-red measurements of ELM filament heat loads indicate that the filament aspect ratio changes to $l_{\wedge}/\, l_{\wedge} \approx 2\pi k\chi_{\wedge}/\, 3qc_{\wedge} \sim 1$ by the time they make contact with the wall, i.e. the filaments appear to change from being poloidally elongated to roughly circular as they travel through the SOL.

Let us briefly comment on the relative pressure perturbation due the ELM filaments, $\Delta p/p_0$. In the "effective" filament approach we may estimate this initial relative perturbation as a ratio of pedestal and separatrix pressures. Assuming that pedestal pressure is determined by the width of the pedestal and that the ideal ballooning limit remains roughly the same for different sized Type-I ELMs, one may expect it to be only weakly dependent of ELM size, i.e. $\Delta p/p_0 \sim p_{ped}/p_{sep} \sim (\Delta W_{ELM}/W_{ped})^{\delta}$, with $0 < \delta < 1$. While this has yet to be experimentally confirmed, one may note that $\Delta W_{ELM}/W_{ped}$ decreases with pedestal collisionality roughly as $\sim \nu_{ped}^{*-0.4}$, where $\nu_{ped}^{*} \sim qRn_{ped}/T_{ped}^{2}$. Assuming that n_{ped} is set by the Greenwald density and ν_{ped}^{*} varies due to T_{ped}, one may write $\nu_{ped}^{*} \propto p_{ped}^{-2}$ and hence $\Delta W_{ELM}/W_{ped} \propto p_{ped}^{8}$, which would give $\delta \sim 1.25$, if $p_{sep} \sim const$. However, the expected increase of p_{sep} with $\Delta W_{ELM}/W_{ped}$ would likely compensate for this rise in p_{ped} giving a much lower, perhaps even negative, δ. Clearly more measurements are required to address this important point.

Combining the above results, one finds a general expression for the interchange scaling of the radial Mach number of ELM filaments,

$$M_{\perp}^{int} \sim \left(\frac{2l \approx^{\gamma} l_{\perp}^{1} l_{\wedge}^{\gamma}}{a/\varepsilon} \frac{p_{ped}}{p_{sep}}\right)^{1/2} \left[2\varepsilon\left(\frac{2\pi}{q}\right)^{1-\gamma} \frac{1}{n_0} \frac{p_{ped}}{p_{sep}}\right]^{1/2} \sim \left[\varepsilon\left(\frac{2\pi}{q}\right)^{1-\gamma} \left(\frac{\Delta W_{ELM}}{W_{ped}}\right)^{1+\delta}\right]^{1/2} \tag{7}$$

where $\varepsilon = a/R$; for default values $\gamma = \delta = 0$ this yields $M_{\perp}^{\text{int}} \sim (2\,\pi\varepsilon/q)^{1/2}(\Delta W_{ELM}/W_{ped})^{1/2}$. Note that the scaling with ELM amplitude is independent of γ, due to the observed constancy of the initial filament aspect ratio, (6). This prediction compares favourably with exponents inferred from measurements on JET using turbulence transport probes [12]: $M_{\perp}^{\text{int}} \sim (\Delta W_{ELM}/W_{ped})^{\alpha}$, $\alpha \sim 0.3$-0.4; the divertor energy deficit [10, 3, 7]: $\alpha \sim 0.3$-0.5; and direct infra-red measurements of heat loads on the outboard limiters, $\alpha \sim 0.4$. This last value is easily derived from the data in Table 2, from [11], by noting that $f_{ELM}^{wall} \sim 5$ and 10 % for $<\Delta W_{ELM}> \sim 250$ and 500kJ, and/or $\Delta W/W_{ped} \sim 0.09$ and 0.18, which yields λ_W^{ELM} of 23mm and 30mm, respectively, and using equation (2) with $M_{\perp}^{\text{int}} \sim (\Delta W/W_{ped})^{\alpha}$ to find $\alpha \approx 0.4$. This value will be adopted below for the extrapolation to ITER.

The above results suggest the interchange scaling (7) slightly overestimates the exponent α, unless the ratio of pedestal and separatrix pressures decreases weakly with ELM amplitude ($\delta \sim -0.2$); at present this ratio has not been accurately measured and we assume that $|\delta| << 1$. More likely, sheath dissipative effects modify the interchange scaling with ELM amplitude, reducing α below $0.5 + \delta$ [4]. The predictions of $M_{\perp}^{\text{int}}$ increasing with μ and decreasing with q, are yet to be tested, although the former is consistent with results from MAST ($\varepsilon < 1$) in which higher $M_{\perp}^{\text{int}}$ int are measured than in convential tokamaks ($\varepsilon < 1/3$) [7]. Finally, equation (7) can also explain why Type-III ELMs deposit far less energy to the wall in terms of the drop in pedestal pressure in the I-III transition, i.e. pped / psep is smaller by roughly a factor of 2 in Type-III compared to Type-I ELMs.

3. ELM FILAMENT HEAT LOADS ON ITER

The JET results may be used to predict the average ELM filament heat loads on the first wall in the reference ITER scenario (4 keV pedestal, $q_{95} \approx 3$). For given values of r and $\Delta W_{ELM}/W_{ped}$, the fraction of ELM energy to the wall on ITER may be approximated to lowest order using equation (2). Extrapolating directly from JET measurements, the perpendicular Mach number and the ELM filament energy width, $\lambda_W^{ELM} \approx L_{//} M_{\perp}^{ELM}$, equation (2), may be estimated as

$$M_{\perp}^{ITER}/0.0016 \approx {}_{w}^{ELM,ITER}(cm)/2 \times 2.5 \quad \left(\frac{3}{q_{95}}\right)^{\frac{1-\gamma}{2}} \left(\frac{\Delta W_{ELM}/W_{ped}}{0.12}\right)^{0.4} \tag{8}$$

which is a generalization of the expression suggested in [Fundamenski07]; in the above we used the JET value of $\lambda_W^{ELM} \sim 3$ cm obtained for $\Delta W_{ELM}/W_{ped} \sim 0.12$ and $q^{95} \approx 3$, as well as the fact that $L_{//} \sim \pi q_{95} R$ is twice as large on ITER than on JET due to the larger major radius.

The fraction of ELM energy reaching the wall in ITER is predicted using these two methods, Fig.5: (i) a simple exponential decay, combining equations (2) and (8), Fig.5(a) and (ii) the parallel loss model with radial velocity scaled according to equation (8), i.e.

$$V_{\perp}^{ITER}(m/s) \quad 600 \quad \left(\frac{2}{0.8}\right)^{1/2} \left(\frac{3}{q_{95}}\right)^{\frac{1-\gamma}{2}} \left(\frac{\Delta W_{ELM}/W_{ped}}{0.12}\right)^{0.4} \tag{9}$$

where the ratio inside the square-root reflects the temperatures at mid-pedestal conditions, 2keV in ITER versus 800eV in JET, Fig.5(b). Here we set $\Delta_{ped}/2$ = 2.5cm, Δ_{SOL} = 5cm to the upper baffle and Δ_{SOL} = 15cm to the outer limiter. The former method predicts $W' \sim 23\%$ and 0.8% reaching the upper baffle for natural (ΔW_{ELM} = 20MJ, W_{ped} = 150MJ, $\Delta W/W_{ped} \sim 13.3\%$) and mitigated ($\Delta W_{ELM}$ = 1MJ, $\Delta W/W_{ped} \sim 0.66\%$) ELMs, respectively, and $W' \sim 3\%$ and ~10-5 reaching the outer limiter, Fig.5(a). The latter, more accurate method, also predicts $W' \sim 25\%$ for the natural ELMs, but a substantially higher value, $W' \sim 4\%$, for the mitigated ELMs at the outer baffle, Fig.5(b). As ever, it should be stressed that, considering both the number of assumptions and the scatter in the available data, the accuracy of the above predictions is difficult to assess, and is probably no better than a factor of 2.

CONCLUSIONS

On the basis of the above analysis one may conclude that ~ 4% and ~ 25% of the ELM energy will reach the main chamber in ITER for mitigated (1MJ) and unmitigated (natural, 20MJ) ELMs, respectively, with the majority deposited on the upper baffle. Provided the smaller value, corresponding to ~ 40kJ/ELM or ~ 800kW (assuming $f_{ELM} \sim 20$Hz) can be tolerated by the Beryllium armour tiles, the maximum ELM size on ITER would be determined by the heat load limits on divertor, rather than main chamber, PFCs.

ACKNOWLEDGEMENTS

This work was funded jointly by the UK Engineering and Physical Sciences Research Council and by the European Communities under the contract of Association between EURATOM and UKAEA. The view and opinions expressed herein do not necessarily reflect those of the European Commission.

REFERENCES

[1]. Beurskens M., et al, these proceedings
[2]. Fundamenski W., et al, *PPCF* (2006)
[3]. Fundamenski W., et al, *J.Nucl.Mater* (2007)
[4]. Fundamenski W., et al, submitted to *J.Nucl.Mater*
[5]. Garcia O.E., et al, *Phys.Plasmas (*2006)
[6]. Jakubowski M., et al, submitted to *J.Nucl.Mater*
[7]. Kirk A., et al, Plasma.Phys.Control.Fusion **49** (2007) 1259
[8]. Loarte A., et al, *EPS (2007)*, prep. PPCF.
[9]. Pitts R.A., et al, Nuclear Fusion (2006)
[10]. Pitts R.A., et al, Nuclear Fusion (2007);
[11]. Pitts R.A., et al, submitted to *J.Nucl.Mater*, preprint as EFDA–JET–CP(08)02/24
[12]. Silva C., private communication.

Experiment	Parallel loss model
Limiter probes + TC $T_e\,(r_{lim})$ ~ 25 – 30eV, $n_e\,(r_{lim})$ ~ 2.4 – 10^{18}m^{-3} $\lambda_{n,max}$ ~ 50mm, $\lambda_{Te,max}$ ~ 30mm Nearly all power found on the divertor	$T_e\,(r_{lim})$ ~ 30eV, $n_e\,(r_{lim})$ ~ 2.2 – 10^{18}m^{-3} $\lambda_{n,max}$ ~ 47mm, $\lambda_{Te,max}$ ~ 32mm Fraction of ELM energy to limiter ~ 5%
Outer gap scan + IR & TC λ_w ~ 33 – 35mm, $\lambda_{w,max}$ ~ 22 – 24mm	λ_w ~ 36mm, $\lambda_{w,max}$ ~ 22mm
RFA measurements of ion energies J_{sat}, I_{coll}, T_e (reproduced by model)	$T_{i,max}\,(r_{lim})$ ~ 100eV, $T_{e,max}\,(r_{lim})$ ~ 40eV, $n_e\,(r_{lim})$ ~ 4.3 × 1018m^{-3} $\lambda_{n,max}$ ~ 48mm, $\lambda_{Ti,max}$ ~ 52mm $\lambda_{Te,max}$ ~ 30mm, λ_w ~ 32mm Fraction of ELM energy to limiter ~ 15%
ELM energy deficit based on IR ~ 30% for ~ 3cm gap and ΔW/W ~ 5%	~ 30% based on $\lambda_W{}^{ELM}$ ~ 35mm

Table 1: Comparison between experimental measurements and parallel loss model predictions of ELM-wall contact on JET in four separate dedicated experiments [3].

Pulse No.	Γ_{gas} (10^{22} e/s)	No. ELMs	$\Sigma\Delta W_{ELM}$ (MJ)	f_{lim} (MJ)	$<\Delta W_{ELM}>$ (kJ)	$f_{lim}{}^{ELM} = \Sigma E_{lim}$ / $\Sigma\Delta W_{ELM} = <E_{lim}>$ / $<\Delta W_{ELM}>$
70221	1.47	133	29.7	1.49	224	5.3
70222	1.24	87	23.9	1.02	275	4.3
70223	0.89	50	18.0	0.85	360	4.7
70224	0.38	16	8.34	0.71	521	8.8
70225	0	30	14.9	1.37	497	9.2
70225	0	24	12.7	1.49	528	11.8

Table 2: Summary of results of a dedicated experiment measuring Type-I ELM heat loads to the outer limiters in six identical discharges with different levels of gas fuelling. Reproduced from [11].

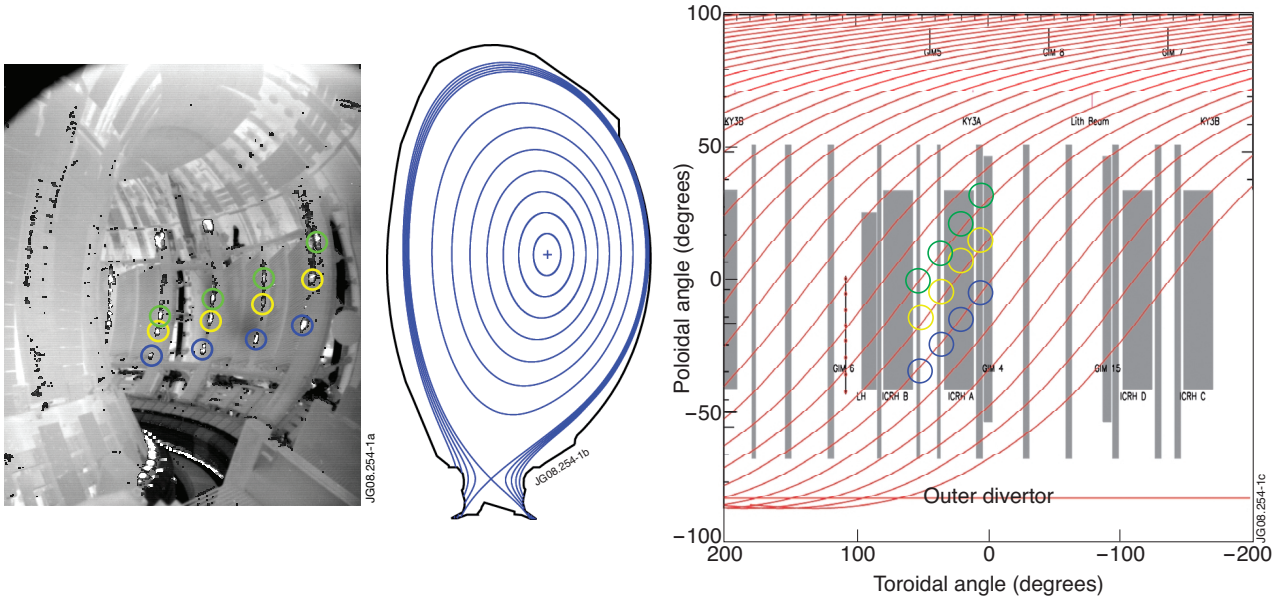

Figure 1: IR image during a Type-I ELM (left), pre-ELM magnetic equilibrium (middle) and ELM-filament footprint and pre-ELM magnetic field (right)[6].

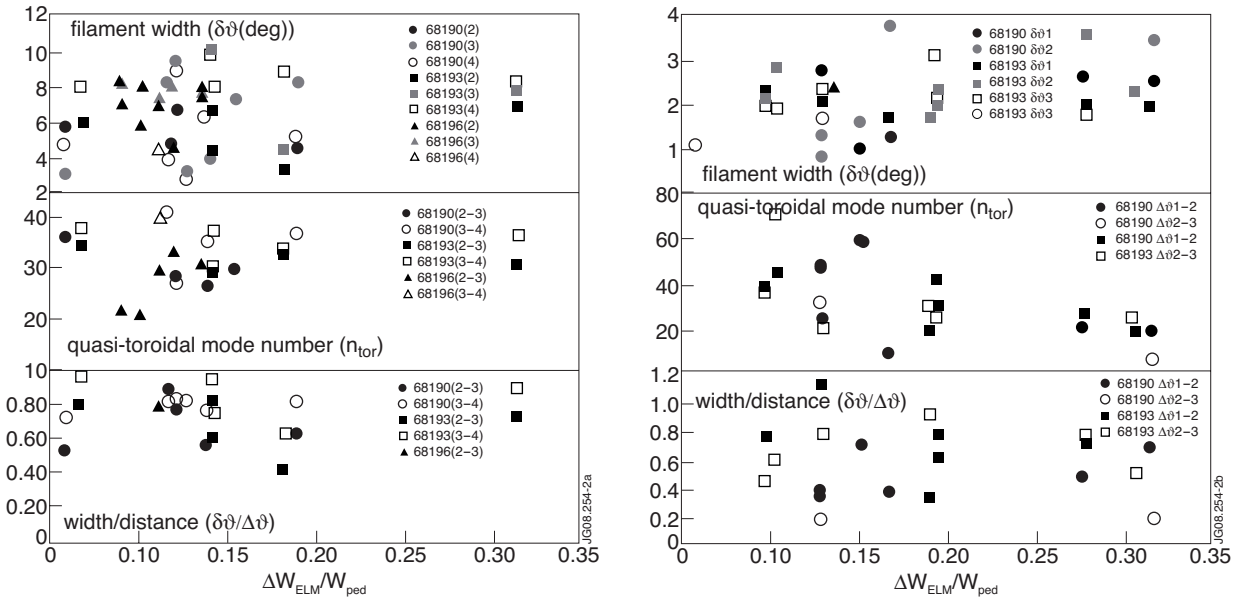

Figure 2: Variation of filament footprints structure with ELM size for the outer limiters (a) and upper dump plates (b): top - footprint width, middle - toroidal mode number at the wall radius, n_w, bottom - fraction of the filament imprint width to the separation of the filaments. Reproduced from [6].